# **Inorganic Chemistry**

pubs.acs.org/IC Article

# Synthesis, Structure, and Properties of Volatile Lanthanide Dialkyltriazenides

Christopher M. Caroff and Gregory S. Girolami\*



Cite This: Inorg. Chem. 2022, 61, 16740-16749



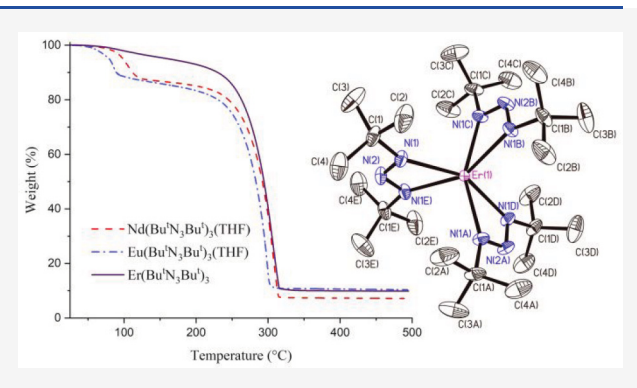
**ACCESS** I

Metrics & More

Article Recommendations

Supporting Information

**ABSTRACT:** Several dialkyltriazenide complexes of the lanthanide elements neodymium, europium, and erbium have been prepared; these include the homoleptic complex  $Er(Bu^tN_3Bu^t)_3$ , the tetrahydrofuran monoadducts  $Ln(Bu^tN_3Bu^t)_3(THF)$  where Ln=Nd or Eu, and the lithium salts  $[Li(THF)][Ln(MeN_3Bu^t)_4]$  where Ln=Eu or Er. Crystal structures, nuclear magnetic resonance data, and infrared data are reported for all complexes. The di-tert-butyltriazenide complexes are thermally stable, sublime at reasonably low temperatures, and show smooth volatilization without decomposition, which make them potentially useful in lanthanide separation processes and as chemical vapor deposition precursors for lanthanide nitrides and other phases.



#### INTRODUCTION

Lanthanide nitrides exhibit a variety of interesting optical, electronic, and magnetic properties that make them promising materials for several technological applications such as spintronics. <sup>1,2</sup> Bulk lanthanide nitrides have been synthesized in a number of ways: by thermal decomposition of europium and ytterbium amides, <sup>3–6</sup> by ammonolysis of homoleptic bis-(trimethylsilyl)amido or cyclopentadienyl lanthanide complexes, <sup>7,8</sup> by salt elimination from lanthanide chlorides and lithium nitride, <sup>9</sup> and more recently by the thermal decomposition of lanthanide complexes bearing nitrogen-rich bis-(tetrazolato)amine ligands. <sup>10</sup> Several methods for the deposition of thin films of lanthanide nitrides have been reported, primarily by physical vapor deposition (PVD) techniques such as molecular beam epitaxy, <sup>11–13</sup> reactive evaporation, <sup>14–16</sup> or pulsed laser deposition. <sup>12,17,18</sup>

In comparison to PVD, chemical vapor deposition (CVD) has several advantages, including a large deposition area, high film uniformity, control over film composition, and the ability to grow conformal coatings or completely fill complex device structures such as trenches with high aspect ratios. <sup>19</sup> CVD processes, however, depend on the availability of precursors that can be vaporized. Many volatile lanthanide compounds are known, <sup>20</sup> but it is difficult to design lanthanide compounds with high vapor pressures because their ionic radii are large. The large radii mean that sterically bulky ligands are needed to saturate the coordinate sphere; the resulting compounds tend to have large molecular surface areas and thus strong intermolecular London attractive forces.

In part because of the scarcity of suitable precursors, there have been only a few reports of the growth of lanthanide nitride thin films by CVD. Some of the more promising precursors for

this purpose are complexes that possess an all-nitrogen coordination environment such as homoleptic lanthanide amidinates and guanidinates;<sup>21-25</sup> such compounds are most likely to afford films that are free of oxygen and carbon impurities. In fact, dysprosium and gadolinium nitride thin films have been grown by CVD from tris(guanidinate) and tris-(amidinate) complexes at deposition temperatures of 650-850 °C; the guanidinato compounds produce lanthanide nitride films under single-source precursor conditions with relatively small amounts of carbon contamination, whereas the amidinato compounds produce lanthanide nitride films at temperatures as low as 450 °C but only when ammonia is used as a coreactant. $^{26-28}$  Despite these advancements, there is a clear need for the development of new lanthanide-containing CVD precursors that are volatile, are reactive at lower temperatures, and do not contain metal-carbon or metal-oxygen bonds.

Closely related to amidinates and guanidinates are the triazenides; in the latter anions, the central carbon atom has been replaced with nitrogen:

Received: July 18, 2022 Published: October 7, 2022





Table 1. Crystallographic Data for Lanthanide Di-tert-butyltriazenide Complexes 1-3

	1	2	3
formula	$C_{28}H_{62}N_9NdO$	$C_{28}H_{62}N_9EuO$	$C_{24}H_{54}ErN_9$
formula weight	685.10	692.82	636.02
temp (K)	100(2)	200(2)	100(2)
λ (deg)	0.71073	0.71073	0.71073
crystal system	monoclinic	monoclinic	trigonal
space group	$P2_1/c$	$P2_1/c$	P321
a (Å)	9.5288(2)	9.6042(2)	17.5161(3)
b (Å)	20.0267(5)	20.3998(3)	17.5161(3)
c (Å)	19.0713(5)	18.6570(3)	9.3281(2)
$\alpha/\beta/\gamma$ (deg)	90/101.005(1)/90	90/98.8894(5)/90	90/90/120
$V(Å^3)$	3572.46(15)	3611.44(11)	2478.55(10)
Z	4	4	3
$ \rho_{\rm calc}  ({\rm g \ cm}^{-3}) $	1.274	1.274	1.278
$\mu \text{ (mm}^{-1})$	1.486	1.769	2.564
F(000)	1444	1456	987
crystal size (mm)	$0.778 \times 0.344 \times 0.182$	$0.283 \times 0.162 \times 0.129$	$0.625 \times 0.442 \times 0.346$
$\theta$ range (deg)	30.541-2.178	28.292-2.282	28.291-2.325
R(int)	0.0392	0.0334	0.0484
Abs corr type	multiscan	multiscan	multiscan
max, min transmission factors	0.5546, 0.7461	0.6304, 0.7457	0.4679, 0.7457
data/restraints/parameters	10920/0/371	8956/63/403	4128/0/179
goodness of fit on F <sup>2</sup>	1.146	1.073	1.071
$R_1 \left[ F_0 > 4\sigma(F_0) \right]^a$	0.0221	0.0213	0.0223
$wR_2$ (all data) <sup>b</sup>	0.0494	0.0523	0.0561
max, min $\Delta \rho_{\rm elect}$ (e Å <sup>-3</sup> )	1.01, -0.70	0.51, -0.57	0.79, -0.68

 ${}^{a}R_{1} = \sum ||F_{o}| - |F_{c}|| / |\sum |F_{o}||$  for reflections, where  $F_{o}^{2} > 2\sigma(F_{o}^{2})$ .  ${}^{b}wR_{2} = [\sum w(F_{o}^{2} - F_{c}^{2})^{2} / \sum (F_{o}^{2})^{2}]^{1/2}$  for all reflections.

Because (other things being equal) the nitrogen content and thermal reactivity of triazenides are higher than that of amidinates and guanidinates, lanthanide triazenides might serve as better CVD precursors and afford lanthanide nitride thin films at lower growth temperatures.

Triazenide complexes of the alkali metals,  $^{29}$  transition metals,  $^{30-33}$  and main group metals  $^{34-37}$  are well-known, and homoleptic triazenide complexes of some main group elements have been used as precursors for the deposition of nitride films by atomic layer deposition (ALD).  $^{38-40}$  Although several lanthanide triazenide complexes are known, all of them contain 1,3-diaryltriazenide ligands,  $^{41-49}$  and the large London forces and  $\pi-\pi$  stacking characteristic of aryl groups render the complexes essentially nonvolatile and thus unsuited for use as CVD precursors. For example, tris(1,3-diphenyltriazenido)bis(pyridine) complexes of erbium and lutetium were studied in the context of vapor deposition, but these complexes decompose before subliming.  $^{41}$ 

Interestingly, there have been no reports of lanthanide complexes of 1,3-dialkyltriazenides, which should be more volatile than similar aryl counterparts. Here we describe the synthesis, structure, and properties of a series of neodymium, europium, and erbium complexes bearing 1,3-dialkyltriazenide ligands of the form  $[RN_3Bu^t]^-$ , where R=Me or  $Bu^t$ . As we will show, several of these compounds have properties that make them potentially useful as precursors for the CVD of lanthanide-containing thin films. In addition to CVD, these compounds may be of interest for other applications such as in separation technology, particularly as it relates to the reprocessing of spent nuclear fuel. <sup>50</sup>

#### RESULTS AND DISCUSSION

Synthesis of Lanthanide Dialkyltriazenide Compounds. The reaction of the anhydrous lanthanide trihalides  $MCl_3$ , where M = Nd, Eu, or Er, with 3 equiv of lithium 1,3-di*tert*-butyltriazenide,  $Li(Bu^tN_3Bu^t)$ , gives the compounds  $Nd-(Bu^tN_3Bu^t)_3(THF)$  (1),  $Eu(Bu^tN_3Bu^t)_3(THF)$  (2), and  $Er-(Bu^tN_3Bu^t)_3$  (3).

$$LnCl_3 + 3Li(Bu^tN_3Bu^t) \xrightarrow{\text{thf}} RT, 20h \xrightarrow{\text{tBu}} V_N \xrightarrow{\text{tBu}} V_$$

Ln = Nd (1) Yield: 47%, Eu (2) Yield: 26%

The reactions to synthesize tetrahydrofuran adducts 1 and 2 were carried out in THF, and the products were crystallized from pentane. The analogous reaction of  $ErCl_3$  with Li- $(Bu^tN_3Bu^t)$  in THF affords a bright orange pentane soluble product that we were unable to crystallize. We found, however, that treatment of  $ErCl_3$  with 3 equiv of  $Li(Bu^tN_3Bu^t)$  in diethyl ether followed by crystallization from pentane gives orange crystals of the THF-free erbium compound,  $Er(Bu^tN_3Bu^t)_3$  (3). Attempts to synthesize the THF-free europium triazenide

**Inorganic Chemistry** Article pubs.acs.org/IC

complex in diethyl ether gave a pentane soluble yellow solid that we were unable to crystallize or sublime. The stoichiometries of all of these products (i.e., whether the complex is preferentially isolated as a THF adduct) are consistent with periodic trends. Ions of the early lanthanides, such as Nd<sup>3+</sup> and Eu<sup>3+</sup>, have larger ionic radii and tend to form complexes with coordination numbers that are higher than those of ions of the later lanthanides, such as Er<sup>3+</sup>, which are smaller.

In an effort to synthesize lanthanide dialkyltriazenide complexes with higher volatilities, we investigated reactions of lanthanide trichlorides with triazenide anions bearing smaller alkyl groups on nitrogen. The reaction of EuCl<sub>3</sub> and ErCl<sub>3</sub> with 3 equiv of lithium methyl-tert-butyltriazenide, Li(MeN<sub>3</sub>Bu<sup>t</sup>), in THF at room temperature does generate isolable compounds, but the products are the ionic tetrakis compounds [Li(THF)]- $[Eu(MeN_3Bu^t)_4]$  (4) and  $[Li(THF)][Er(MeN_3Bu^t)_4]$  (5), which can be isolated as red-orange and light-orange crystals, respectively, after crystallization from pentane.

$$LnCl_3 + 4Li(MeN_3Bu^t) \xrightarrow[RT,20~h]{THF} \underbrace{[Li(THF)][Ln(MeN_3Bu^t)_4] + 3LiCl}_{Ln=Eu(4)Yield:62\%,Er(5)Yield:36\%}$$

The steric bulk of the methyl-tert-butyltriazenide ligand is small enough that four of them can be accommodated in the coordination sphere; the ionic nature of the compounds means that they are not volatile.

All five of the new dialkyl triazenide compounds are highly soluble in tetrahydrofuran, diethyl ether, toluene, and pentane, even the two ionic salts.

Crystal Structures of the New Lanthanide Dialkyltriazenide Compounds. Crystal data for the new lanthanide dialkyltriazenide complexes are listed in Tables 1 and 2. Complexes 1 and 2, which are isomorphous, crystallize in space group  $P2_1/c$  with one molecule (residing on a general position) per asymmetric unit; selected bond distances and angles are listed in Tables 3 and 4. In both complexes, the lanthanide atom is bound to three chelating triazenide anions and one THF ligand; the seven atoms bound to the Ln atom form a distorted pentagonal bipyramid (Figures 1 and 2). In the Nd complex, 1, the Nd-N distances range between 2.45 and 2.57 Å: presumably because of steric repulsion, the four nitrogen atoms closest to the THF molecule (i.e., those having smaller O-Nd-N angles) form the longest contacts of 2.52-2.57 Å. The Nd-O distance is 2.50 Å. In Eu complex 2, the geometry is similar but the metal-ligand bonds are 0.03-0.06 Å shorter than the corresponding bonds in Nd complex 1. This difference correlates well with the approximately 0.03-0.05 Å difference in ionic radius between Nd<sup>5+</sup> and Eu<sup>3+</sup>. S1 As a result of the different ionic radii, the average N-Ln-N bite angle of the triazenide ligands is slightly larger in 2 (52.0°) than in 1 (51.3°).

THF-free Er complex 3 crystallizes in trigonal space group P321 with one molecule residing on a site of 32 crystallographic symmetry and another molecule residing on a site of 3-fold crystallographic symmetry (adding up to half a molecule per asymmetric unit); the two independent molecules have similar geometries, and selected bond distances and angles are listed in Table 5. The metal atom is bound to three chelating triazenide ligands in which the six metal-bound nitrogen atoms describe a distorted octahedron (Figure 3). The average Er-N distance in 3 is 2.33 Å, which is shorter by 0.09 and 0.13 Å than even the shortest of the Ln-N distances in 1 and 2, respectively. The latter difference correlates well with the change in the ionic radius of 0.12 Å between seven-coordinate Eu<sup>3+</sup> and sixcoordinate Er3+.51 The average bite angle of the triazenide

Table 2. Crystallographic Data for Lanthanide Methyl-tertbutyltriazenide Complexes 4 and 5

	4	5
formula	$C_{24}H_{56}EuLiN_{12}O$	$C_{24}H_{56}ErLiN_{12}O$
formula weight	687.70	703.00
temp (K)	100(2)	100(2)
λ (deg)	0.71073	0.71073
crystal system	monoclinic	monoclinic
space group	$P2_1/n$	$P2_1/n$
a (Å)	11.0412(2)	10.9648(3)
b (Å)	17.9475(4)	17.8083(6)
c (Å)	18.0768(4)	18.0227(6)
$\beta$ (deg)	102.1085(5)	101.6762(10)
$V(Å^3)$	3502.44(13)	3446.37(19)
Z	4	4
$ ho_{ m calc}$ (g cm <sup>-3</sup> )	1.304	1.355
$\mu \text{ (mm}^{-1}\text{)}$	1.825	2.470
F(000)	1432	1452
crystal size (mm)	$0.222 \times 0.156 \times 0.096$	$0.197 \times 0.13 \times 0.107$
$\theta$ range (deg)	28.288-2.201	28.305-2.308
R(int)	0.0377	0.0436
Abs corr type	multiscan	multiscan
max, min transmission factors	0.6762, 0.7457	0.6651, 0.7457
data/restraints/ parameters	8683/0/388	8569/51/388
goodness of fit on $F^2$	1.063	1.053
$R_1 \left[ F_0 > 4\sigma(F_0) \right]^a$	0.0147	0.0178
$wR_2$ (all data) <sup>b</sup>	0.0356	0.0388
max, min $\Delta \rho_{ m elect}$ (e Å $^{-3}$ )	0.42, -0.42	0.42, -0.37
${}^{a}R_{1} = \sum_{r}   F_{0}  -  F_{c}   /  \sum_{r}  F_{0}  = \frac{1}{2}   F_{0}   /  \sum_{r}  F_{0}   /  F_{0}   / $	$ F_0 $ for reflections, wher	$e F_o^2 > 2\sigma(F_o^2)$ . $^b w F_o^2$

=  $[\sum w(F_o^2 - F_c^2)^2 / \sum (F_o^2)^2]^{1/2}$  for all reflections.

ligands in 3 is 55.7°; this angle is larger than the bite angles measured for 1 and 2 and consistent with the smaller size of the Er<sup>3+</sup> ion.

The M-N bond distances in complexes 1-3 are generally similar to those reported for Nd, Eu, and Er guanidinate and amidinate complexes with similar steric properties. 21,23,52 The Er-N distances of 2.320(5)-2.348(4) Å in 3 are insignificantly shorter than those of 2.350(14)-2.408(11) and 2.354(3)-2.360(3) Å in the amidinate  $\text{Er}(\text{Bu}^{t}\text{NCMeNBu}^{t})_{3}^{23}$  and the guanidinate Er[Pr<sup>i</sup>NC(NMe<sub>2</sub>)NPr<sup>i</sup>]<sub>3</sub>,<sup>52</sup> respectively. Despite the similar Er-N bond distances, the ligand bite angles in 3 are smaller (by  $\sim 1.5^{\circ}$ ) than those in the amidinate Er-(ButNCMeNBut)3, because of the shorter N-N bonds in the backbone of the triazenide ligand in 3 versus the longer N-C bonds in the backbone of the amidinate ligand. The average N-N-N ligand backbone angle in 3 of  $111(1)^{\circ}$  is identical to the N-C-N angle seen in this latter amidinate complex.

1-Methyl-3-tert-butyltriazenide complexes 4 and 5, which are isomorphous, crystallize in space group  $P2_1/n$  with one molecule (residing on a general position) in the asymmetric unit; selected bond distances and angles are listed in Tables 6 and 7. Unlike the tris(di-tert-butyltriazenide) complexes 1-3, in 4 and 5, the lanthanide centers are bound to four chelating triazenide ligands; a Li(THF) cation balances the charge (Figures 4 and 5). The eight nitrogen atoms of the four chelating triazenide ligands delineate a  $D_{2d}$  dodecahedron about the lanthanide center. The lithium ion binds to three nitrogen atoms of two of the triazenide ligands and is also bound to one THF molecule, giving a distorted tetrahedral environment about lithium. The ability of four triazenide ligands to coordinate to the metal center in 4 and

Table 3. Selected Bond Distances and Angles for Nd(Bu<sup>t</sup>N<sub>3</sub>Bu<sup>t</sup>)<sub>3</sub>(THF)

	Distan	nces (Å)	
Nd(1)-N(1)	2.5348(13)	Nd(1)-N(7)	2.4813(13)
Nd(1)-N(2)	2.9489(13)	Nd(1)-N(8)	2.9921(13)
Nd(1)-N(3)	2.4540(13)	Nd(1)-N(9)	2.5711(13)
Nd(1)-N(4)	2.5209(13)	Nd(1) - O(1)	2.4995(11)
Nd(1)-N(5)	3.013(13)		
Nd(1)-N(6)	2.5470(13)		
	Angle	s (deg)	
O(1)-Nd(1)-N(1)	85.59(4)	N(1)-Nd(1)-N(3)	51.87(4)
O(1)-Nd(1)-N(3)	137.28(4)	N(4)-Nd(1)-N(6)	50.77(4)
O(1)-Nd(1)-N(4)	100.43(4)	N(7)-Nd(1)-N(9)	51.16(4)
O(1)-Nd(1)-N(6)	78.50(4)	N(1)-N(2)-N(3)	113.44(12)
O(1)-Nd(1)-N(7)	119.93(4)	N(4)-N(5)-N(6)	112.29(12)
O(1)-Nd(1)-N(9)	89.42(4)	N(7)-N(8)-N(9)	113.62(12)

Table 4. Selected Bond Distances and Angles for  $Eu(Bu^tN_3Bu^t)_3(THF)$ 

, , , , , ,	•		
Distances (Å)			
Eu(1)-N(1)	2.5138(16)	Eu(1)-N(7)	2.5017(15)
Eu(1)-N(2)	2.9241(16)	Eu(1)-N(8)	2.9689(15)
Eu(1)-N(3)	2.4253(16)	Eu(1)-N(9)	2.4804(16)
Eu(1)-N(4)	2.4892(16)	Eu(1) - O(1)	2.4630(15)
Eu(1)-N(5)	2.9316(13)		
Eu(1)-N(6)	2.4620(16)		
	Angle	s (deg)	
O(1)-Eu(1)-N(1)	84.84(6)	N(1)-Eu(1)-N(3)	52.34(6)
O(1)-Eu(1)-N(3)	137.17(6)	N(4)-Eu(1)-N(6)	52.29(5)
O(1)-Eu(1)-N(4)	89.77(5)	N(7)-Eu(1)-N(9)	51.43(5)
O(1)-Eu(1)-N(6)	122.12(6)	N(1)-N(2)-N(3)	113.45(16)
O(1)-Eu(1)-N(7)	77.18(5)	N(4)-N(5)-N(6)	113.88(15)
O(1)-Eu(1)-N(9)	93.50(6)	N(7)-N(8)-N(9)	112.22(15)

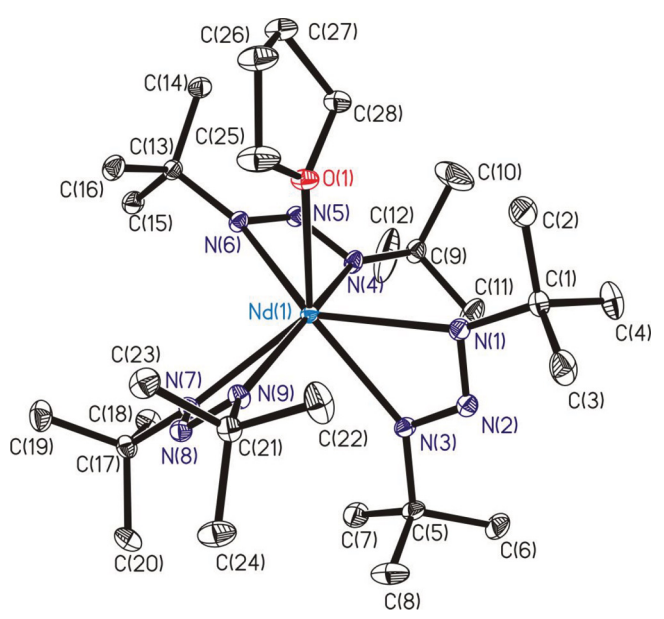
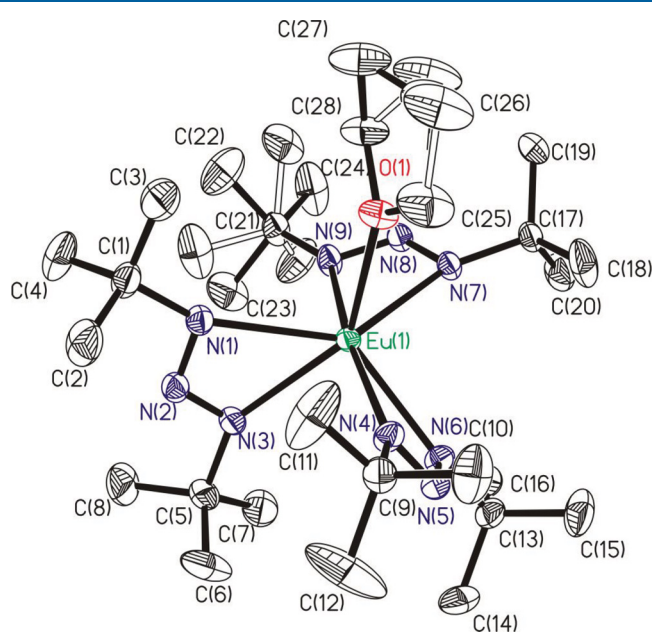


Figure 1. ORTEP representation of  $Nd(Bu^tN_3Bu^t)_3(THF)$  (1). Ellipsoids are drawn at the 35% probability level. Hydrogen atoms have been omitted for the sake of clarity.

5 is indicative of the decreased steric profile of the methyl-*tert*-butyltriazenide ligand relative to the di-*tert*-butyltriazenide ligand in complexes 1–3.



**Figure 2.** ORTEP representation of Eu(Bu<sup>t</sup>N<sub>3</sub>Bu<sup>t</sup>)<sub>3</sub>(THF) (2). Ellipsoids are drawn at the 35% probability level. Hydrogen atoms have been omitted for the sake of clarity.

The Eu-N distances in 4 range between 2.43 and 2.50 Å for the nitrogen atoms that bind to only europium; this range is similar to that observed in di-tert-butyltriazenide europium complex 2. The three nitrogen atoms in 4 that bind to both europium and lithium have longer Eu-N distances of 2.55, 2.56, and 2.59 Å. The bite angles of the triazenide ligands in 4 are between 49.3° and 52.5°. The two ligands that do not bind to the lithium ion have larger bite angles, both between 52.3 and 52.5°, consistent with their shorter Eu-N distances; the ligands that bind both europium and lithium have correspondingly smaller bite angles of 49.3 and 50.4°. In 5, the Er-N distances and the ligand bite angles show similar behavior, except that the Ln-N distances in 5 are shorter by ~0.06 Å as expected from the difference in ionic radius between eight-coordinate Eu<sup>3+</sup> and  $\mathrm{Er}^{3+.51}$  The ligand bite angles in 5 (53.6° for the triazenide ligands that do not bind to lithium and  $50.5^{\circ}$  and  $51.6^{\circ}$  for the other two triazenide ligands), are all slightly larger than those in 4 due to the shorter M–N bond lengths.

**Spectroscopic Properties.** The <sup>1</sup>H nuclear magnetic resonance (NMR) spectra of the electrically neutral Nd, Eu,

Table 5. Selected Bond Distances and Angles for Er(Bu<sup>t</sup>N<sub>3</sub>Bu<sup>t</sup>)<sub>3</sub>

	Distar	nces (Å)		
$\operatorname{Er}(1)$ - $\operatorname{N}(1)$	2.331(4)	Er(2)-N(21)	2.320(5)	
$\operatorname{Er}(1) - \operatorname{N}(1)'$	2.331(4)	Er(2)-N(21)'	2.320(5)	
$\operatorname{Er}(1) - \operatorname{N}(1)''$	2.331(4)	Er(2)-N(21)''	2.320(5)	
Er(1)-N(1)'''	2.331(4)	Er(2)-N(22)	2.811(5)	
$\operatorname{Er}(1) - \operatorname{N}(1)^{\dagger}$	2.331(4)	Er(2)-N(22)'	2.811(5)	
$\text{Er}(1) - \text{N}(1)^{\ddagger}$	2.331(4)	Er(2)-N(22)''	2.811(5)	
$\operatorname{Er}(1)$ - $\operatorname{N}(2)$	2.806(5)	Er(2)-N(23)	2.348(4)	
Er(1)-N(2)'	2.806(5)	Er(2)-N(23)'	2.348(4)	
Er(1)-N(2)''	2.806(5)	Er(2)-N(23)"	2.348(4)	
Angles (deg)				
$N(1)-Er(1)-N(1)^{\ddagger}$	55.52(18)	N(21)-Er(2)-N(23)	55.8(2)	
N(1)-Er(1)-N(1)''	105.04(11)	N(21)-Er(2)-N(21)'	106.56(14)	
$N(1)-Er(1)-N(1)^{\dagger}$	152.6(2)	N(21)-Er(2)-N(23)'	153.9(2)	
N(1)-Er(1)-N(1)'	105.04(11)	N(21)-Er(2)-N(21)''	106.56(14)	
N(1)-Er(1)-N(1)'''	99.2(2)	N(21)-Er(2)-N(23)''	97.6(2)	
$N(1)-N(2)-N(1)^{\ddagger}$	111.2(5)	N(21)-N(22)-N(23)	110.9(4)	
<sup>a</sup> Symmetry transformations used to gene	erate equivalent atoms: ', -y, x	-y, z; ", -x + y, -x, z; "", y, x, -z; †, x	$-y, -y, -z; \stackrel{:}{:}, -x, -x + y, -z$	

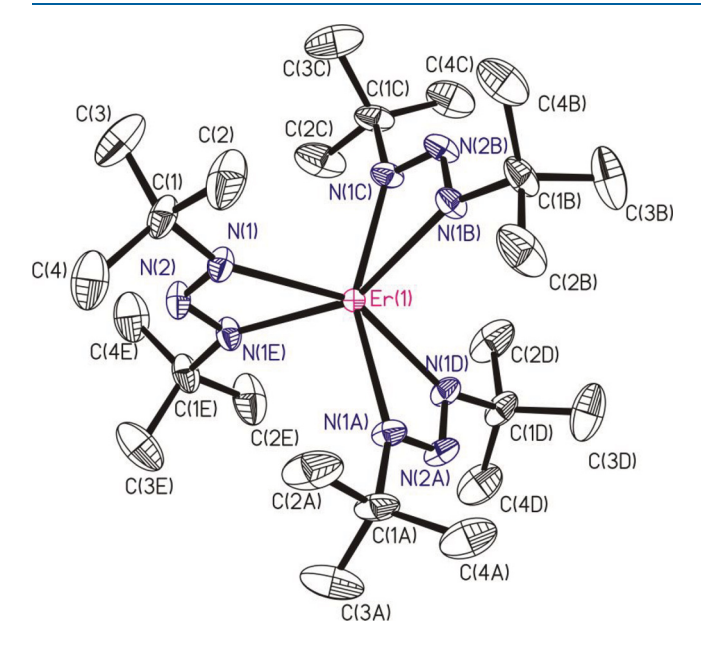


Figure 3. ORTEP representation of one of the two independent molecules of  $Er(Bu^tN_3Bu^t)_3$  (3). Ellipsoids are drawn at the 35% probability level. Hydrogen atoms have been omitted for the sake of clarity.

and Er compounds 1–3 feature a paramagnetically broadened and shifted resonance due to the *tert*-butyl groups of the triazenide ligands at  $\delta$  0.39, 2.69, and 5.59, respectively. In complexes 1 and 2, two additional resonances at  $\delta$  0.75 and 0.19 for 1 and  $\delta$  3.68 and 1.47 for 2 are also observed for the bound THF molecule. The <sup>1</sup>H NMR spectrum of Er salt 5 shows a resonance for the *tert*-butyl substituent at  $\delta$  18.21 and a resonance for the methyl substituent at  $\delta$  –87.61, in addition to resonances for the THF groups at  $\delta$  9.79 and 2.65. The <sup>1</sup>H NMR spectrum of the Eu salt 4 is similar, but the shifts due to the paramagnetism are smaller.

In the 1970s, it had been proposed that the various binding modes of the triazenide ligand (unidentate, chelating, and bridging) can often be distinguished by infrared (IR) spectroscopy: N–N stretching absorptions generally appear between 1190–1210 and 1260–1300 cm<sup>-1</sup> for unidentate triazenide

ligands, 1260–1300 cm<sup>-1</sup> for chelating triazenide ligands, and 1350–1375 cm<sup>-1</sup> for bridging triazenide ligands.<sup>53–58</sup> These correlations were based on studies of platinum–metal coordination complexes, and more recent data suggest that they are not particularly useful outside this class of compounds.<sup>33,59</sup> The IR spectra of 1–5 also suggest that the correlations above are not universal: there are several strong N–N stretching absorptions between 1200 and 1357 cm<sup>-1</sup>, which span the reported ranges of all three binding modes, even though the triazenide ligands in all five compounds are clearly chelating as determined crystallographically. No peaks in the range of 3200–3300 cm<sup>-1</sup> corresponding to N–H groups of neutral triazenes were observed in the IR spectra.

Thermal Properties and Volatility. When heated as solids in closed capillaries under 1 atm of argon, THF adducts 1 and 2 change color (green to yellow-green for 1 and red to dark red for 2) at 80–100 °C and release THF (evident as a condensate on the cooler parts of the capillary). When heated further, 1 darkens above 280 °C whereas 2 melts at 292 °C and subsequently darkens. Complex 3 undergoes no visible changes until it is heated to 280 °C, at which point it begins to darken without melting.

As part of determining the suitability of the new lanthanide triazenide complexes as precursors for CVD and ALD, and potentially in separations technology, we carried out more quantitative studies of the volatility of 1-3 under 1 atm of nitrogen by thermogravimetric analysis (TGA) at ramp rates of 10 °C/min (Figure 6). For all three compounds, smooth volatilization is observed with no obvious thermal decomposition below 300 °C. The TGA curves of 1 and 2 are very similar, showing two clear weight loss steps: one step between 70 and 90 °C (mass loss of 10−12%) that we attribute to the loss of bound THF and a second step at higher temperatures due to volatilization of the THF-free complex. For this latter step, the onset of volatilization (at ~279 and ~272 °C) and the temperature at which volatilization is complete (~300 and  $\sim$ 310 °C) are very similar for the two compounds. In contrast to the TGA curves of 1 and 2, that for the THF-free complex 3 shows only one weight loss step, with the onset of volatilization occurring at 273 °C and the temperature at which volatilization is complete being 310 °C. The agreement of these latter temperatures with those seen for the second weight loss step in 1

Table 6. Selected Bond Distances and Angles for [Li(THF)][Eu(MeN<sub>3</sub>Bu<sup>t</sup>)<sub>4</sub>] (4)

	Distan	ces (Å)	
Eu(1)-N(1)	2.4338(10)	Eu(1)-N(10)	2.5615(10)
Eu(1)-N(2)	2.9171(11)	Eu(1)-N(11)	2.9396(10)
Eu(1)-N(3)	2.4738(11)	Eu(1)-N(12)	2.4988(11)
Eu(1)-N(4)	2.4441(11)	Li(1)-N(7)	2.172(3)
Eu(1)-N(5)	2.9181(11)	Li(1)-N(9)	2.104(3)
Eu(1)-N(6)	2.4589(11)	Li(1)-N(10)	2.075(3)
Eu(1)-N(7)	2.5456(11)	Li(1) - O(1)	1.892(3)
Eu(1)-N(8)	2.9582(11)		
Eu(1)-N(9)	2.5867(11)		
	Angles	s (deg)	
N(1)-Eu(1)-N(3)	52.37(4)	N(7)-N(8)-N(9)	109.13(10)
N(4)-Eu(1)-N(6)	52.47(4)	N(10)-N(11)-N(12)	110.51(10)
N(7)-Eu(1)-N(9)	49.32(4)		
N(10)-Eu(1)-N(12)	50.41(3)		
N(1)-N(2)-N(3)	111.80(10)		
N(4)-N(5)-N(6)	111.76(11)		

Table 7. Selected Bond Distances and Angles for [Li(THF)][Er(MeN<sub>3</sub>Bu<sup>t</sup>)<sub>4</sub>] (5)

	Distan	ces (Å)	
Er(1)-N(1)	2.3725(13)	Er(1)-N(10)	2.4983(13)
$\operatorname{Er}(1) - \operatorname{N}(2)$	2.8609(14)	Er(1)-N(11)	2.9033(14)
Er(1)-N(3)	2.4137(14)	Er(1)-N(12)	2.4408(14)
Er(1)-N(4)	2.3785(14)	Li(1)-N(7)	2.183(3)
Er(1)-N(5)	2.8634(14)	Li(1)-N(9)	2.109(3)
Er(1)-N(6)	2.4033(14)	Li(1)-N(10)	2.065(3)
Er(1)-N(7)	2.4820(15)	Li(1)-O(1)	1.888(3)
$\operatorname{Er}(1) - \operatorname{N}(8)$	2.9213(15)		
$\operatorname{Er}(1) - \operatorname{N}(9)$	2.5311(14)		
	Angle	s (deg)	
N(1)-Er(1)-N(3)	53.57(5)	N(7)-N(8)-N(9)	109.19(14)
N(4)-Er(1)-N(6)	53.58(5)	N(10)-N(11)-N(12)	110.26(13)
N(7)-Er(1)-N(9)	50.54(5)		
N(10)-Er(1)-N(12)	51.62(5)		
N(1)-N(2)-N(3)	111.33(14)		
N(4)-N(5)-N(6)	111.16(14)		

and 2 further supports the conclusion that the first weight loss step in 1 and 2 is due to the loss of THF.

In a dynamic vacuum ( $\sim$ 0.01 Torr), compounds 1–3 sublime slowly between 60 and 80 °C and relatively rapidly at 90–120 °C. Under the conditions studied, 1 and 2 sublime with partial but not complete loss of THF. A comparison of the volatility of 1–3 with those of similar lanthanide amidinates and guanidinates is reported in Table 8.

These data suggest that 1-3 are more volatile than amidinate and guanidinate complexes with the same tert-butyl substituents on the terminal atoms of the ligand backbone, probably because 1-3 lack substituents on the central atom of the backbone. Compounds 1-3 have volatilities that are in the same range as those of lanthanide amidinates and guanidinates that bear terminal isopropyl groups and small substituents (Me or NMe<sub>2</sub>) on the central atom.

## CONCLUSIONS

We have synthesized a series of lanthanide complexes bearing chelating di-tert-butyltriazenide and methyl-tert-butyltriazenide ligands. The di-tert-butyltriazenide complexes of neodymium, europium, and erbium are thermally stable, sublime at reasonably low temperatures, and show smooth volatilization

without decomposition (except for loss of bound THF molecules). The smaller steric profile of the methyl-tert-butyltriazenide ligand affords ionic tetrakis lanthanide complexes [Li(THF)][Ln(MeN\_3Bu^t)\_4] (Ln = Eu or Er) that are not volatile. The crystal structures show that the triazenide ligands (as expected) bind to lanthanide ions in a fashion similar to that seen for chemically related amidinate and guanidinate ligands, except that the bite angles are slightly smaller in the triazenides because of the shorter N–N–N backbone.

Our findings suggest that lanthanide triazenide complexes may be useful as precursors for the deposition of thin films of lanthanide nitrides by CVD techniques. In addition, as mentioned in the introduction, although extractions and chromatographic methods are most often employed to separate and purify f-block elements in their +3 oxidation states, f it may be possible to separate f-metals on the basis of the differential volatilities of their triazenide complexes, as has been demonstrated for certain f-diketonate complexes.

# EXPERIMENTAL SECTION

All experiments were carried out under vacuum or under argon by using standard Schlenk techniques. Solvents were distilled under nitrogen from sodium/benzophenone immediately before use. Anhydrous

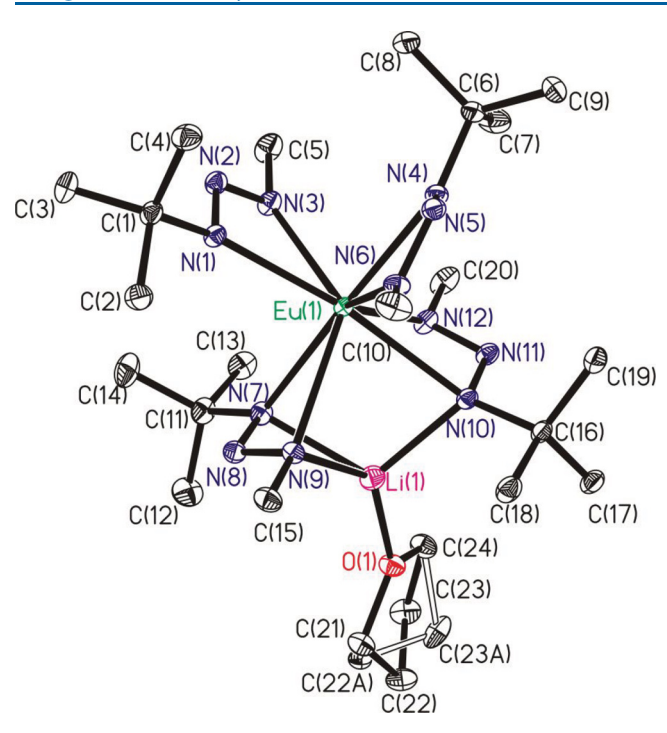


**Figure 4.** ORTEP representation of [Li(THF)][Eu(MeN<sub>3</sub>Bu<sup>t</sup>)<sub>4</sub>] (4). Ellipsoids are drawn at the 35% probability level. Hydrogen atoms have been omitted for the sake of clarity.

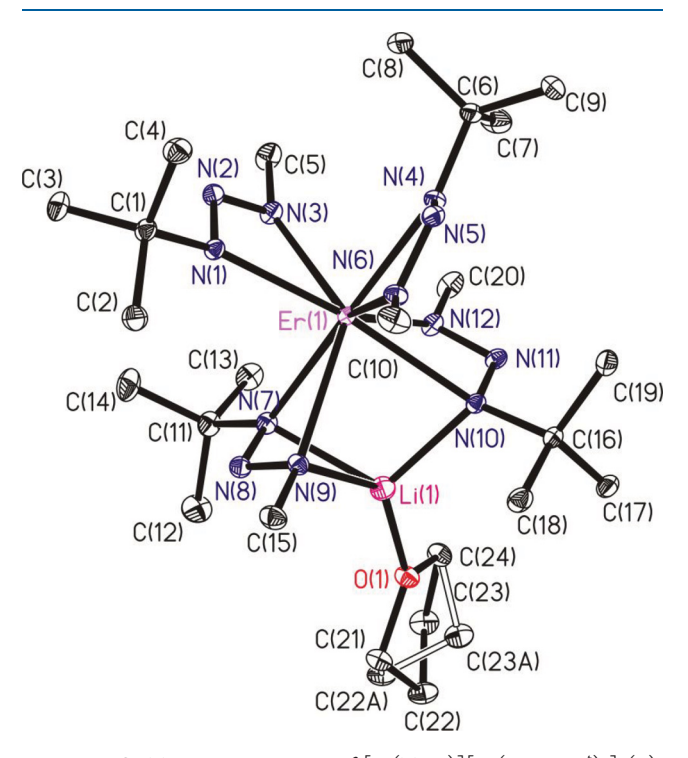


**Figure 5.** ORTEP representation of  $[\text{Li}(\text{THF})][\text{Er}(\text{MeN}_3\text{Bu}^t)_4]$  (5). Ellipsoids are drawn at the 35% probability level. Hydrogen atoms have been omitted for the sake of clarity.

NdCl<sub>3</sub>, EuCl<sub>3</sub>, and ErCl<sub>3</sub> were purchased from Strem and used as received. Compounds Li(Bu<sup>t</sup>N<sub>3</sub>Bu<sup>t</sup>)<sup>36</sup> and Li(MeN<sub>3</sub>Bu<sup>t</sup>)<sup>63</sup> were prepared by literature routes. Microanalyses were performed by the University of Illinois Microanalytical Laboratory using combustion techniques. <sup>1</sup>H NMR data were collected on a Varian Unity Inova spectrometer at 400 MHz; chemical shifts are reported in  $\delta$  units (positive chemical shifts to higher frequency) relative to tetramethylsi-

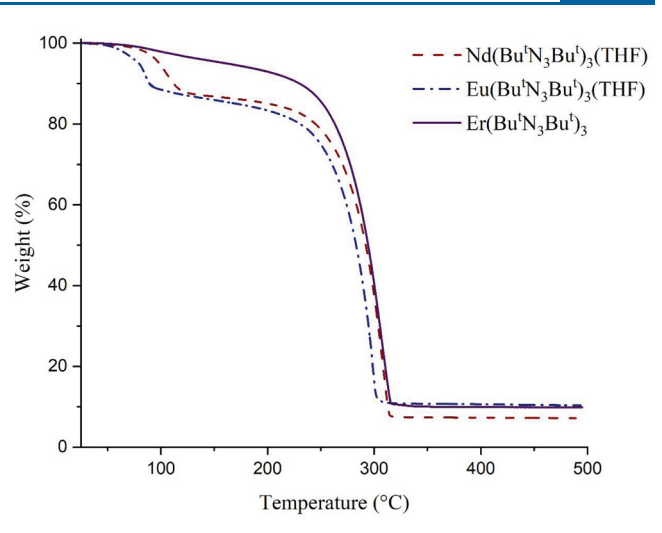


Figure 6. TGA plots for lanthanide triazenides 1-3 under 1 atm of nitrogen at ramp rates of  $10~^{\circ}\text{C/min}$ .

Table 8. Vacuum Sublimation Temperatures and Vaporization Onset Temperatures at 1 atm (from TGA curves) of 1–3 Along with Data for Related Lanthanide Amidinato (AMD) and Guanidinato (guan) Complexes

	$T_{\text{subl}}$ (°C) in vacuum	$T_{\mathrm{vap}}$ (°C) at 1 atm
$Nd(N_3tBu_2)_3(THF)$ (1)	120	270
$Eu(N_3tBu_2)_3(THF)$ (2)	120	270
$Er(N_3tBu_2)_3$ (3)	120	270
$\operatorname{Ln}({}^{i}\operatorname{Pr-Me-AMD})_{3}^{23,27,60}$	80-140	210-225
$Ln(^tBu-Me-AMD)_3^{23}$	220	not available
$\operatorname{Ln}({}^{i}\operatorname{Pr-}c-\operatorname{C}_{2}\operatorname{H}_{4}\operatorname{-}\operatorname{AMD})_{3}^{52}$	150-200	not available
$\operatorname{Ln}(i\operatorname{Pr-Me}_{2}\operatorname{N-guan})_{3}^{21,22,27}$	120-135	220-240
Ln( <sup>i</sup> Pr-Et <sub>2</sub> N-guan) <sub>3</sub> <sup>22</sup>	150-165	229 <sup>a</sup>
$\operatorname{Ln}({}^{i}\operatorname{Pr-}{}^{i}\operatorname{Pr}_{2}\operatorname{N-guan})_{3}^{22}$	not available	238 <sup>a</sup>
$\operatorname{Ln}({}^{i}\operatorname{Pr-}c-\operatorname{C}_{2}\operatorname{H}_{4}-\operatorname{guan})_{3}^{52}$	150-200	not available

<sup>&</sup>lt;sup>a</sup>Multiple weight loss steps and high residual mass.

lane (TMS). The IR spectra were recorded on a Nicolet Impact 410 instrument as Nujol mulls between KBr plates.

Caution: Catenated nitrogen compounds often present explosion hazards. Although we have not experienced any problems in the synthesis, characterization, sublimation, or handling of the compounds described here, their energetic properties have not been fully investigated and therefore they should be handled using standard safety precautions for explosive materials (safety glasses, face shield, blast shield, puncture resistant gloves, and ear protection).

Tris(1,3-di-tert-butyltriazenido)(tetrahydrofuran)neodymium(III), Nd(Bu<sup>t</sup>N<sub>3</sub>Bu<sup>t</sup>)<sub>3</sub>(THF) (1). To a suspension of NdCl<sub>3</sub> (0.26 g, 1.04 mmol) in THF (20 mL) at 0 °C was added a solution of lithium di-tert-butyltriazenide (0.567 g, 3.48 mmol) in THF (20 mL) dropwise. The yellow-green mixture was warmed to room temperature and stirred for 20 h to afford a bright green solution. The solvent was removed under vacuum, and the sticky green residue was extracted with pentane (30 mL). The green extract was filtered, and the filtrate was concentrated under vacuum to ~10 mL and cooled to −20 °C. The resulting green-brown plates were collected by filtration and dried under vacuum. Yield: 0.338 g (47%). Anal. Calcd for C<sub>28</sub>H<sub>62</sub>N<sub>9</sub>NdO: C, 49.2; H, 9.12; N, 18.4. Found: C, 49.2; H, 9.15; N, 18.0. <sup>1</sup>H NMR  $(C_6D_6, 20 \,^{\circ}C)$ :  $\delta 0.75$  (br, fwhm = 47 Hz, 4H,  $\alpha$ -CH<sub>2</sub>), 0.39 (s, fwhm = 16 Hz, 54H, CMe<sub>3</sub>), 0.19 (br, fwhm = 28 Hz, 4H,  $\beta$ -CH<sub>2</sub>). IR (cm<sup>-1</sup>): 1356 m, 1287 s, 1243 m, 1198 s, 1064 w, 1047 w, 1028 w, 914 w, 891 w, 750 w. 619 m.

Tris(1,3-di-tert-butyltriazenido)(tetrahydrofuran)europium-(III), Eu(Bu $^t$ N $_3$ Bu $^t$ )(THF) (2). To a suspension of EuCl $_3$  (0.310 g, 1.20 mmol) in THF (15 mL) at 0 °C was added a solution of lithium di-tert-

butyltriazenide (0.571 g, 3.50 mmol) in THF (15 mL) dropwise. The brown-red mixture was warmed to room temperature and stirred for 20 h to afford a dark red solution. The solvent was removed under vacuum, and the sticky red solid was extracted with pentane (50 mL). The dark red extract was filtered, and the filtrate was concentrated under vacuum to ~10 mL and cooled to  $-20\,^{\circ}\text{C}$ . The resulting dark red prisms were collected by filtration and dried in vacuum. Yield: 175 mg (26%). Anal. Calcd for  $C_{28}H_{62}N_9\text{EuO}$ : C, 48.5; H, 9.02; N, 18.2. Found: C, 48.4; H, 9.08; N, 17.6.  $^1\text{H}$  NMR (C<sub>6</sub>D<sub>6</sub>, 20  $^{\circ}\text{C}$ ):  $\delta$  3.68 (br, fwhm = 68 Hz, 4H,  $\alpha$ -CH<sub>2</sub>), 2.69 (s, fwhm = 6 Hz, 54H, CMe<sub>3</sub>), 1.47 (br, fwhm = 38 Hz, 4H,  $\beta$ -CH<sub>2</sub>). IR (cm $^{-1}$ ): 1356 m, 1284 s, 1267 s, 1245 s, 1200 s, 1078 w, 1065 w, 1028 w, 980 w, 920 w, 868 w, 750 w, 617 m.

Tris(1,3-di-tert-butyltriazenido)erbium(III), Er(Bu<sup>t</sup>N<sub>3</sub>Bu<sup>t</sup>)<sub>3</sub> (3). To a suspension of ErCl<sub>3</sub> (0.22 g, 0.80 mmol) in diethyl ether (20 mL) at 0 °C was added a solution of lithium di-tert-butyltriazenide (0.420 g, 2.58 mmol) in diethyl ether (20 mL) dropwise. The orange mixture was warmed to room temperature and stirred for 20 h to give an orange solution. The solvent was removed under vacuum, and the sticky orange solid was extracted with pentane (40 mL). The extract was filtered, and the filtrate was concentrated under vacuum to ~10 mL and cooled to -20 °C. The resulting orange prisms were collected by filtration and dried in vacuum. Yield: 200 mg (40%). Anal. Calcd for C<sub>24</sub>H<sub>54</sub>N<sub>9</sub>Er: C, 45.3; H, 8.56; N, 19.8. Found: C, 45.3; H, 8.58; N, 19.3. <sup>1</sup>H NMR (C<sub>6</sub>D<sub>6</sub>, 20 °C): δ 5.59 (s, fwhm = 110 Hz, 54H, CMe<sub>3</sub>). IR (cm<sup>-1</sup>): 1357 m, 1336 w, 1267 s, 1246 s, 1203 s, 1086 w, 1056 w, 1036 w, 1030 w, 899 w, 885 w, 754 w, 619 m.

Lithium(tetrahydrofuran) Tetrakis(1-methyl-3-tertbutyltriazenido)europate(III), [Li(THF)][Eu(MeN<sub>3</sub>Bu<sup>t</sup>)<sub>4</sub>] (4). To a suspension of EuCl<sub>3</sub> (0.22 g, 0.85 mmol) in THF (15 mL) at 0 °C was added a solution of lithium methyl-tert-butyltriazenide (0.30 g, 2.5 mmol) in THF (15 mL) dropwise. The mixture was warmed to room temperature and stirred for 20 h to give a red-orange solution. The solvent was removed under vacuum, and the sticky orange solid was extracted with pentane (50 mL). The red-orange extract was filtered, and the filtrate was concentrated under vacuum to ~15 mL and cooled to -20 °C. The resulting red-orange prisms were collected by filtration and dried in vacuum. Yield: 265 mg (62%). Anal. Calcd for C<sub>24</sub>H<sub>56</sub>N<sub>12</sub>EuLiO: C, 41.9; H, 8.21; N, 24.4. Found: C, 41.8; H, 8.14; N, 23.9.  $^{1}$ H NMR ( $C_{6}D_{6}$ , 20  $^{\circ}$ C):  $\delta$  5.0 (br, fwhm = 700 Hz), 4.10 (br, fwhm = 38 Hz, 4H,  $\alpha$ -CH<sub>2</sub>), 1.66 (br, fwhm = 24 Hz, 4H,  $\beta$ -CH<sub>2</sub>), 1.50 (br, fwhm = 700 Hz). IR (cm<sup>-1</sup>): 1408 w, 1355 m, 1286 s, 1243 m, 1214 s, 1155 w, 1070 w, 1037 m, 919 w, 887 w, 804 w, 723 w, 683 w, 611 m, 560 w, 505 m.

Lithium(tetrahydrofuran) Tetrakis(1-methyl-3-tertbutyltriazenido)erbate(III), [Li(THF)][Er(MeN<sub>3</sub>Bu<sup>t</sup>)<sub>4</sub>] (5). To a suspension of ErCl<sub>3</sub> (0.29 g, 1.06 mmol) in THF (15 mL) at 0 °C was added a solution of lithium methyl-tert-butyltriazenide (0.40 g, 3.3 mmol) in THF (15 mL) dropwise. The orange solution was warmed to room temperature and stirred for 20 h. The solvent was removed under vacuum, and the sticky pale-orange solid was extracted with pentane (50 mL). The pale-orange extract was filtered, and the filtrate was concentrated under vacuum to  ${\sim}15$  mL and cooled to  ${-}20$   ${^{\circ}\text{C}}.$  The resulting pale-orange prisms were collected by filtration and dried in vacuum. Yield: 210 mg (36%). Anal. Calcd for C<sub>24</sub>H<sub>56</sub>N<sub>12</sub>ErLiO: C<sub>2</sub> 41.0; H, 8.03; N, 23.9. Found: C, 40.6; H, 8.02; N, 23.1. <sup>1</sup>H NMR  $(C_6D_6, 20 \,^{\circ}C)$ :  $\delta$  18.21 (br, fwhm = 2000 Hz, 36H, CMe<sub>3</sub>), 9.79 (br, fwhm = 370 Hz, 4H,  $\alpha$ -CH<sub>2</sub>), 2.65 (br, fwhm = 570 Hz, 4H,  $\beta$ -CH<sub>2</sub>), -87.61 (br, fwhm = 2100 Hz, 12H, NMe). IR (cm<sup>-1</sup>): 1412 w, 1355 m, 1295 s, 1245 m, 1217 s, 1072 w, 1036 m, 918 w, 887 m, 787 w, 723 w, 684 w, 614 m, 562 w, 505 m.

Thermogravimetric Studies. TGA experiments were performed with a TA Instruments Q50 analyzer on Pt sample pans. The TGA instrument was operated under ambient conditions and not inside a glovebox. As a result, additional sample preparation steps were taken to limit the exposure of these air- and moisture-sensitive complexes to the atmosphere during the sample loading process. Samples were prepared in an argon-filled glovebox in hermetically sealed DSC sample pans that had been preweighed on an analytical balance; the mass of the pans was subtracted from the total mass recorded by the instrument during measurements to calculate the sample mass. Immediately before the

sample was loaded into the TGA instrument, the DSC pans were punctured with several holes, approximately 1 mm in diameter, that were large enough that volatilization would not be diffusion limited and free volatilization of the complexes could occur. For ramp experiments, the  $10{-}20~\text{mg}$  samples were heated under a flow of  $N_2$  to  $500~^\circ\text{C}$  at a rate of  $10~^\circ\text{C}/\text{min}$ . The onset of volatilization was measured as the intersection of the tangents of the initial plateau and the point in the TGA curve at which the mass loss rate is greatest.

The residual masses of 7% (1), 10% (2), and 10% (3) for these compounds are likely attributable to hydrolysis during transfer of the sample to the instrument, despite the precautions taken. If the residual mass were due to thermal decomposition, then it should change in proportion to the sample mass employed. In contrast, we found that doubling the sample mass does not change the final residual mass significantly  $(\pm 0.2 \text{ mg})$ .

General Crystallographic Procedure. The following details were common to all of the crystal structure determinations; for details about individual compounds, see section 3 of the Supporting Information. Crystals mounted on Nylon loops with Krytox oil were transferred onto the diffractometer and kept at a low temperature in a cold nitrogen gas stream. Intensity data were collected on a Bruker Apex II diffractometer equipped with a CCD detector. Standard peak search and indexing procedures gave rough cell dimensions. Data were collected with an area detector by using the measurement parameters listed in Tables 1 and 2. The measured intensities were reduced to structure factor amplitudes and their estimated standard deviations by correction for background, scan speed, and Lorentz and polarization effects. No corrections for crystal decay were necessary, but an appropriate absorption correction was applied. Systematically absent reflections were deleted, and symmetry-equivalent reflections were averaged to yield the set of unique data. The structure was solved by Patterson, direct, or intrinsic phasing methods (OLEX); subsequent least-squares refinement and difference Fourier calculations revealed the positions of all of the non-hydrogen atoms. The analytical approximations to the scattering factors were used, and all of the structure factors were corrected for both real and imaginary components of anomalous dispersion. Hydrogen atoms were placed in idealized positions; methyl groups were allowed to rotate about the C-C axis to find the best leastsquares positions. The displacement parameters for methylene and methine hydrogens were set equal to  $1.2 U_{\rm eq}$  for the attached carbon; those for methyl hydrogens were set to  $1.5 U_{\mathrm{eq}}$ . In the final cycle of least squares, independent anisotropic displacement factors were refined for the non-hydrogen atoms. Final refinement parameters are listed in Tables 1 and 2. A final analysis of variance between observed and calculated structure factors showed no apparent errors.

# ASSOCIATED CONTENT

# Supporting Information

The Supporting Information is available free of charge at https://pubs.acs.org/doi/10.1021/acs.inorgchem.2c02545.

Crystallographic studies, TGA plots, <sup>1</sup>H NMR spectra, and IR spectra for all compounds (PDF)

# **Accession Codes**

CCDC 2190375—2190379 contain the supplementary crystallographic data for this paper. These data can be obtained free of charge via <a href="www.ccdc.cam.ac.uk/data\_request/cif">www.ccdc.cam.ac.uk/data\_request/cif</a>, or by emailing <a href="data\_request@ccdc.cam.ac.uk">data\_request/cif</a>, or by contacting The Cambridge Crystallographic Data Centre, 12 Union Road, Cambridge CB2 1EZ, UK; fax: +44 1223 336033.

# AUTHOR INFORMATION

# **Corresponding Author**

Gregory S. Girolami — School of Chemical Sciences, University of Illinois at Urbana-Champaign, Urbana, Illinois 61801, United States; ⊚ orcid.org/0000-0002-7295-1775; Email: ggirolam@illinois.edu

#### **Author**

Christopher M. Caroff — School of Chemical Sciences, University of Illinois at Urbana-Champaign, Urbana, Illinois 61801, United States

Complete contact information is available at: https://pubs.acs.org/10.1021/acs.inorgchem.2c02545

#### Notes

The authors declare no competing financial interest.

# ACKNOWLEDGMENTS

The authors thank the U.S. Department of Energy (DOE), Office of Science, Office of Basic Energy Science, Separation Science, via Grant DESC0019021 and the National Science Foundation for support of this work under Grant CHE 19-54745 (both to G.S.G.). The authors thank Dr. Danielle Gray and Dr. Toby Woods of the G. L. Clark Laboratory for collecting the X-ray diffraction data and the NMR laboratory and the microanalytical laboratory of the School of Chemical Sciences at the University of Illinois at Urbana-Champaign for assistance with data collection. The authors thank Dr. Roddel Remy for assistance in collecting TGA data. This work was carried out in part in the Materials Research Laboratory Central Research Facilities, University of Illinois at Urbana-Champaign.

# REFERENCES

- (1) Aerts, C. M.; Strange, P.; Horne, M.; Temmerman, W. M.; Szotek, Z.; Svane, A. Half-Metallic to Insulating Behavior of Rare-Earth Nitrides. *Phys. Rev. B: Condens. Matter* **2004**, *69*, 045115.
- (2) Duan, C.-G.; Sabirianov, R. F.; Mei, W. N.; Dowben, P. A.; Jaswal, S. S.; Tsymbal, E. Y. Electronic, Magnetic and Transport Properties of Rare-Earth Monopnictides. *J. Phys.: Condens. Matter* **2007**, *19*, 315220.
- (3) Imamura, H.; Imahashi, T.; Zaimi, M.; Sakata, Y. Preparation and Characteristics of Various Rare Earth Nitrides. *J. Alloys Compd.* **2008**, 451, 636–639.
- (4) Imamura, H.; Sakata, Y.; Nuruyu, T.; Imahashi, T. Preparation and Properties of Nanocrystalline Ytterbium and Europium Nitride (YbN and EuN). *J. Alloys Compd.* **2006**, *418*, 251–254.
- (5) Howell, K.; Pytlewski, L. L. The Decomposition Products of Solutions of Europium and Ytterbium Metals in Liquid Ammonia. *Journal of the Less Common Metals* **1969**, *19*, 399–404.
- (6) Juza, R.; Hadenfeldt, C. Darstellung und Eigenschaften von Europium(II)-amid. *Die Naturwissenschaften* **1968**, *55*, 229–229.
- (7) Baisch, U.; Pagano, S.; Zeuner, M.; Barros, N.; Maron, L.; Schnick, W. Nanocrystalline Lanthanide Nitride Materials Synthesised by Thermal Treatment of Amido and Ammine Metallocenes: X-ray Studies and DFT Calculations. Chem. Eur. J. 2006, 12, 4785–4798.
- (8) LaDuca, R. L.; Wolczanski, P. T. Preparation of Lanthanide Nitrides via Ammonolysis of Molten {(Me<sub>3</sub>Si)<sub>2</sub>N}<sub>3</sub>Ln: Onset of Crystallization Catalyzed by Lithium Amide and Lithium Chloride. *Inorg. Chem.* **1992**, *31*, 1311–1313.
- (9) Fitzmaurice, J. C.; Hector, A.; Rowley, A. T.; Parkin, I. P. Rapid, Low Energy Synthesis of Lanthanide Nitrides. *Polyhedron* **1994**, *13*, 235–240.
- (10) Nguyen, T.-A. D.; Veauthier, J. M.; Chavez, D. E.; Tappan, B. C.; Mueller, A. H.; Scott, B. L.; Parrish, D. A. Lanthanide Complexes of Bis(tetrazolato)amine: A Route to Lanthanide Nitride Foams. *Inorg. Chem.* **2020**, *59*, 16109–16116.
- (11) Gerlach, J. W.; Mennig, J.; Rauschenbach, B. Epitaxial Gadolinium Nitride Thin Films. *Appl. Phys. Lett.* **2007**, *90*, 061919.
- (12) Natali, F.; Ludbrook, B.; Galipaud, J.; Plank, N.; Granville, S.; Preston, A.; Do, B. L.; Richter, J.; Farrell, I.; Reeves, R.; Durbin, S.; Trodahl, J.; Ruck, B. Epitaxial Growth and Properties of GdN, EuN and SmN Thin Films. *Phys. Status Solidi C* **2012**, *9*, 605–608.

- (13) Scarpulla, M. A.; Gallinat, C. S.; Mack, S.; Speck, J. S.; Gossard, A. C. GdN (111) Heteroepitaxy on GaN (0001) by  $N_2$  Plasma and  $NH_3$  Molecular Beam Epitaxy. *J. Cryst. Growth* **2009**, *311*, 1239–1244.
- (14) Holmes-Hewett, W. F.; Buckley, R. G.; Ruck, B. J.; Natali, F.; Trodahl, H. J. 4f Conduction in the Magnetic Semiconductor NdN. *Phys. Rev. B: Condens. Matter* **2019**, *100*, 195119.
- (15) McKenzie, W. R.; Munroe, P. R.; Budde, F.; Ruck, B. J.; Granville, S.; Trodahl, H. J. TEM Characterisation of GdN Thin Films. *Curr. Appl. Phys.* **2006**, *6*, 407–410.
- (16) McNulty, J. F.; Temst, K.; Van Bael, M. J.; Vantomme, A.; Anton, E. M. Epitaxial Growth of (100)-Oriented SmN Directly on (100)Si Substrates. *Phys. Rev. Materials* **2021**, *5*, 113404.
- (17) Ludbrook, B. M.; Farrell, I. L.; Kuebel, M.; Ruck, B. J.; Preston, A. R. H.; Trodahl, H. J.; Ranno, L.; Reeves, R. J.; Durbin, S. M. Growth and Properties of Epitaxial GdN. *J. Appl. Phys.* **2009**, *106*, 063910.
- (18) Ruck, B. J.; Trodahl, H. J.; Richter, J. H.; Cezar, J. C.; Wilhelm, F.; Rogalev, A.; Antonov, V. N.; Le, B. D.; Meyer, C. Magnetic State of EuN: X-Ray Magnetic Circular Dichroism at the Eu M<sub>4,5</sub> and L<sub>2,3</sub> Absorption Edges. *Phys. Rev. B: Condens. Matter* **2011**, 83, 174404.
- (19) Abelson, J. R.; Girolami, G. S. New Strategies for Conformal, Superconformal, and Ultrasmooth Films by Low Temperature Chemical Vapor Deposition. *J. Vac. Sci. Technol.*, A **2020**, 38, 030802.
- (20) Drozdov, A.; Kuzmina, N. 2.19 Volatile Compounds of Lanthanides. In *Comprehensive Inorganic Chemistry II*, 2nd ed.; Reedijk, J., Poeppelmeier, K., Eds.; Elsevier: Amsterdam, 2013; pp 511–534.
- (21) Milanov, A. P.; Xu, K.; Cwik, S.; Parala, H.; de los Arcos, T.; Becker, H.-W.; Rogalla, D.; Cross, R.; Paul, S.; Devi, A. Sc<sub>2</sub>O<sub>3</sub>, Er<sub>2</sub>O<sub>3</sub>, and Y<sub>2</sub>O<sub>3</sub> Thin Films by MOCVD from Volatile Guanidinate Class of Rare-Earth Precursors. *Dalton Trans.* **2012**, *41*, 13936–13947.
- (22) Milanov, A. P.; Fischer, R. A.; Devi, A. Synthesis, Characterization, and Thermal Properties of Homoleptic Rare-Earth Guanidinates: Promising Precursors for MOCVD and ALD of Rare-Earth Oxide Thin Films. *Inorg. Chem.* **2008**, *47*, 11405–11416.
- (23) Päiväsaari, J.; Dezelah, C. L., IV; Back, D.; El-Kaderi, H. M.; Heeg, M. J.; Putkonen, M.; Niinistö, L.; Winter, C. H. Synthesis, Structure and Properties of Volatile Lanthanide Complexes Containing Amidinate Ligands: Application for Er<sub>2</sub>O<sub>3</sub> Thin Film Growth by Atomic Layer Deposition. *J. Mater. Chem.* **2005**, *15*, 4224–4233.
- (24) de Rouffignac, P.; Park, J.-S.; Gordon, R. G. Atomic Layer Deposition of  $Y_2O_3$  Thin Films from Yttrium Tris(N,N'-diisopropylacetamidinate) and Water. *Chem. Mater.* **2005**, *17*, 4808–4814.
- (25) Edelmann, F. T. Lanthanide Amidinates and Guanidinates: From Laboratory Curiosities to Efficient Homogeneous Catalysts and Precursors for Rare-Earth Oxide Thin Films. *Chem. Soc. Rev.* **2009**, 38, 2253–2268.
- (26) Milanov, A. P.; Thiede, T. B.; Devi, A.; Fischer, R. A. Homoleptic Gadolinium Guanidinate: A Single Source Precursor for Metal—Organic Chemical Vapor Deposition of Gadolinium Nitride Thin Films. *J. Am. Chem. Soc.* **2009**, *131*, 17062—17063.
- (27) Thiede, T. B.; Krasnopolski, M.; Milanov, A. P.; de los Arcos, T.; Ney, A.; Becker, H.-W.; Rogalla, D.; Winter, J.; Devi, A.; Fischer, R. A. Evaluation of Homoleptic Guanidinate and Amidinate Complexes of Gadolinium and Dysprosium for MOCVD of Rare-Earth Nitride Thin Films. *Chem. Mater.* **2011**, 23, 1430–1440.
- (28) Krasnopolski, M.; Hrib, C. G.; Seidel, R. W.; Winter, M.; Becker, H.-W.; Rogalla, D.; Fischer, R. A.; Edelmann, F. T.; Devi, A. Homoleptic Gadolinium Amidinates as Precursors for MOCVD of Oriented Gadolinium Nitride (GdN) Thin Films. *Inorg. Chem.* **2013**, *52*, 286–296.
- (29) Gantzel, P.; Walsh, P. J. Synthesis and Crystal Structures of Lithium and Potassium Triazenide Complexes. *Inorg. Chem.* **1998**, *37*, 3450–3451.
- (30) Moore, D. S.; Robinson, S. D. Catenated Nitrogen Ligands Part I. Transition Metal Derivatives of Triazenes, Tetrazenes, Tetrazadienes, and Pentazadienes. *Adv. Inorg. Chem.* **1986**, *30*, 1–68.
- (31) Gómez, M.; Muller, G.; Sales, J. Synthesis and Characterization of Triazenido and Amidino Complexes of Nickel and Palladium. *Polyhedron* **1993**, *12*, 1171–1177.

- (32) Albertin, G.; Antoniutti, S.; Bedin, M.; Castro, J.; Garcia-Fontán, S. Synthesis and Characterization of Triazenide and Triazene Complexes of Ruthenium and Osmium. *Inorg. Chem.* **2006**, *45*, 3816–3825.
- (33) Guzei, I. A.; Liable-Sands, L. M.; Rheingold, A. L.; Winter, C. H. Synthesis and Characterization of Titanium and Zirconium Complexes Bearing Diphenyltriazenido Ligands. *Polyhedron* **1997**, *16*, 4017–4022.
- (34) Leman, J. T.; Braddock-Wilking, J.; Coolong, A. J.; Barron, A. R. 1,3-Diaryltriazenido Compounds of Aluminum. *Inorg. Chem.* **1993**, 32, 4324–4336.
- (35) Leman, J. T.; Barron, A. R.; Ziller, J. W.; Kren, R. M. Synthesis of 1,3-Diphenyltriazenide Complexes of Aluminium, Gallium and Indium: Crystal Structure of Tris(1,3-diphenyltriazenido)aluminium-(III). *Polyhedron* 1989, 8, 1909–1912.
- (36) Samii, R.; Zanders, D.; Fransson, A.; Bačić, G.; Barry, S. T.; Ojamäe, L.; Kessler, V.; Pedersen, H.; O'Brien, N. J. Synthesis, Characterization, and Thermal Study of Divalent Germanium, Tin, and Lead Triazenides as Potential Vapor Deposition Precursors. *Inorg. Chem.* **2021**, *60*, 12759–12765.
- (37) Samii, R.; Zanders, D.; Buttera, S. C.; Kessler, V.; Ojamäe, L.; Pedersen, H.; O'Brien, N. J. Synthesis and Thermal Study of Hexacoordinated Aluminum(III) Triazenides for Use in Atomic Layer Deposition. *Inorg. Chem.* **2021**, *60*, 4578–4587.
- (38) O'Brien, N. J.; Rouf, P.; Samii, R.; Rönnby, K.; Buttera, S. C.; Hsu, C.-W.; Ivanov, I. G.; Kessler, V.; Ojamäe, L.; Pedersen, H. In Situ Activation of an Indium(III) Triazenide Precursor for Epitaxial Growth of Indium Nitride by Atomic Layer Deposition. *Chem. Mater.* **2020**, 32, 4481–4489.
- (39) Rouf, P.; Samii, R.; Rönnby, K.; Bakhit, B.; Buttera, S. C.; Martinovic, I.; Ojamäe, L.; Hsu, C.-W.; Palisaitis, J.; Kessler, V.; Pedersen, H.; O'Brien, N. J. Hexacoordinated Gallium(III) Triazenide Precursor for Epitaxial Gallium Nitride by Atomic Layer Deposition. *Chem. Mater.* 2021, 33, 3266–3275.
- (40) Rouf, P.; Palisaitis, J.; Bakhit, B.; O'Brien, N. J.; Pedersen, H. In0.5Ga0.5N Layers by Atomic Layer Deposition. *J. Mater. Chem. C* **2021**, *9*, 13077–13080.
- (41) Pfeiffer, D.; Guzei, I. A.; Liable-Sands, L. M.; Heeg, M. J.; Rheingold, A. L.; Winter, C. H. Synthesis, Structure, and Characterization of Lanthanide Complexes Bearing 1,3-Diphenyltriazenido Ligands. *J. Organomet. Chem.* **1999**, 588, 167–175.
- (42) Kolybalov, D. S.; Sukhikh, T. S.; Bashirov, D. A.; Konchenko, S. N. Synthesis and Structure of New Er(III) Complexes With N,N'-1,3-Bis(2,6-diisopropylphenyl)triazenide. *J. Struct. Chem.* **2021**, *62*, 277–284.
- (43) Hauber, S.-O.; Niemeyer, M. Stabilization of Unsolvated Europium and Ytterbium Pentafluorophenyls by  $\pi$ -Bonding Encapsulation through a Sterically Crowded Triazenido Ligand. *Inorg. Chem.* **2005**, *44*, 8644–8646.
- (44) Liu, B.; Cui, D. Rare-Earth Metal Complexes Stabilized by Amino-Phosphine Ligand. Reaction with Mesityl Azide and Catalysis of the Cycloaddition of Organic Azides and Aromatic Alkynes. *Dalton Trans.* **2009**, 550–556.
- (45) Hauber, S.-O.; Woo Seo, J.; Niemeyer, M. Halogenomercury Salts of Sterically Crowded Triazenides Convenient Starting Materials for Redox-Transmetallation Reactions. *Z. Anorg. Allg. Chem.* **2010**, *636*, 750–757.
- (46) Lee, H. S.; Niemeyer, M. Homoleptic Heavy Alkaline Earth and Europium Triazenides. *Inorg. Chem.* **2010**, *49*, 730–735.
- (47) Litlabø, R.; Lee, H. S.; Niemeyer, M.; Törnroos, K. W.; Anwander, R. Rare-Earth Metal Bis(tetramethylaluminate) Complexes Supported by a Sterically Crowded Triazenido Ligand. *Dalton Trans.* **2010**, 39, 6815–6825.
- (48) Turner, Z. R.; Bellabarba, R.; Tooze, R. P.; Arnold, P. L. Addition-Elimination Reactions across the M–C Bond of Metal N-Heterocyclic Carbenes. *J. Am. Chem. Soc.* **2010**, *132*, 4050–4051.
- (49) Gyton, M. R. Diaryl Triazenides as Ligands for the Lanthanides and Related Studies. The University of New South Wales, Sydney, Australia, 2015.

- (50) World Nuclear Association. Processing of Used Nuclear Fuel. https://world-nuclear.org/information-library/nuclear-fuel-cycle/fuel-recycling/processing-of-used-nuclear-fuel.aspx (accessed 2022-07-09).
- (51) Shannon, R. Revised Effective Ionic Radii and Systematic Studies of Interatomic Distances in Halides and Chalcogenides. *Acta Crystallogr. Sect. A: Found. Crystallogr.* **1976**, 32, 751–767.
- (52) Tutacz, P.; Harmgarth, N.; Zörner, F.; Liebing, P.; Hilfert, L.; Engelhardt, F.; Busse, S.; Edelmann, F. T. Two Series of New Volatile Rare-Earth Metal Tris(guanidinates) and Tris(amidinates). Z. Anorg. Allg. Chem. 2018, 644, 1653–1659.
- (53) Kuyper, J.; Van Vliet, P. I.; Vrieze, K. Metal-Metal Bonded Triazenido Compounds: II. Compounds  $[(Ph_3P)_2(CO)M-Ag(R-N-N-R')X]$  with  $M=Rh^I$ ,  $Ir^I$ ; R=Me, aryl and X=Cl, Br, I. *J. Organomet. Chem.* 1976, 105, 379–387.
- (54) Kuyper, J.; van Vliet, P. I.; Vrieze, K. Metal-Metal Bonded Triazenido Compounds: I. Complexes  $[L_2(CO)MCu(R-N-N-R)X]$  with  $M = Rh^I$ ,  $Ir^I$ ;  $L = AsR_3$ ,  $PR_3$ ; R = Me, Aryl and X = Cl, Br, I. J. Organomet. Chem. 1975, 96, 289–299.
- (55) Pfeiffer, E.; Oskam, A.; Vrieze, K. Fluxional Nickel(II)- and Palladium (II)-triazenido ( $C_5H_5$ )(L)(RN<sub>3</sub>R)M Complexes; Evidence for a Triplet-State Intermediate. *Transition Met. Chem.* **1977**, 2, 240–246.
- (56) Knoth, W. H. Triazene Complexes of Group VIII Metals. *Inorg. Chem.* 1973, 12, 38–44.
- (57) Robinson, S. D.; Uttley, M. F. 1,3-Diaryltriazenido Derivatives of the Platinum Metals. *J. Chem. Soc. D* **1971**, 1315–1316.
- (58) Laing, K. R.; Robinson, S. D.; Uttley, M. F. Complexes of the Platinum Metals. Part IV. 1,3-Diaryltriazenido Derivatives. *J. Chem. Soc., Dalton Trans.* 1974, 1205–1214.
- (59) Soussi, K.; Mishra, S.; Jeanneau, E.; Millet, J.-M. M.; Daniele, S. Asymmetrically Substituted Triazenes as Poor Electron Donor Ligands in the Precursor Chemistry of Iron(ii) for Iron-Based Metallic and Intermetallic Nanocrystals. *Dalton Trans.* **2017**, *46*, 13055–13064.
- (60) Lim, B. S.; Rahtu, A.; de Rouffignac, P.; Gordon, R. G. Atomic Layer Deposition of Lanthanum Aluminum Oxide Nano-Laminates for Electrical Applications. *Appl. Phys. Lett.* **2004**, *84*, 3957–3959.
- (61) Gupta, C. K.; Krishnamurthy, N. Extractive Metallurgy of Rare Earths; CRC Press: Boca Raton, FL, 2005.
- (62) Sievers, R. E. Gas Chromatographic and Related Studies of Metal Complexes. In *Coordination Chemistry: Papers Presented in Honor of Professor John C. Bailar, Jr.*; Kirschner, S., Ed.; Springer US: Boston, 1969; pp 270–288.
- (63) Smith, R. H.; Wladkowski, B. D.; Mehl, A. F.; Cleveland, M. J.; Rudrow, E. A.; Chmurny, G. N.; Michejda, C. J. 1,3-Dialkyltriazenes: Tautomeric Equilibria and Rates and Products of Decomposition. *J. Org. Chem.* 1989, 54, 1036–1042.